

# Pressure calibration to 20 GPa by simultaneous use of ultrasonic and x-ray techniques

Baosheng Li<sup>a)</sup> and Jennifer Kung

*Mineral Physics Institute, Stony Brook University, Stony Brook, New York 11794-2100*

Takeyuki Uchida and Yanbin Wang

*Center for Advanced Radiation Sources, The University of Chicago, Chicago, Illinois 60637*

(Received 20 December 2004; accepted 11 May 2005; published online 7 July 2005)

Simultaneous measurements of elastic  $P$ - and  $S$ -wave travel times, density (specific volume), and sample length using a multianvil apparatus interfaced with ultrasonic interferometry and x-ray diffraction and radiography have enabled simultaneous determination of elastic properties and absolute pressure at high pressures and high temperatures. Experimental procedures and data analyses are demonstrated using data collected on polycrystalline samples of ferropicalase ( $\text{MgFe}$ ) and wadsleyite  $\text{Mg}_2\text{SiO}_4$  under quasihydrostatic conditions up to 20 GPa. Compared with those derived from the internal pressure standard in the same experiments based on equations of state of NaCl, the directly determined pressure at 20 GPa is  $\sim 8\%$  and  $\sim 12\%$  higher than those inferred from the Brown and Decker pressure scales, respectively. The discrepancy cannot be reconciled by uncertainties in the NaCl pressure scale and current experimental data. Until further results are available, the pressure determined in this study is believed to be a more accurate measurement of the effective pressure imposed on the sample than that inferred from NaCl based on previous pressure scales. © 2005 American Institute of Physics. [DOI: 10.1063/1.1946905]

## I. INTRODUCTION

Methods for the determination of pressure in various high-pressure devices include fixed-point calibration based on phase transformations of metals and semiconductors (e.g., Bi, Ba, ZnTe, ZnS, and GaAs),<sup>1</sup> and continuous pressure calibration based upon changes in resistance (e.g., manganin),<sup>2</sup> unit-cell volume (e.g., NaCl, Au, Pt, and MgO),<sup>3-5</sup> and ruby-fluorescent lines. Among the increased applications of multianvil apparatus with synchrotron x-radiation source, NaCl is probably the most widely used internal pressure standard in high-pressure research due to the availability of the large body of experimental data as well as a continuous effort to update and refine the scale.<sup>3-5</sup> In general, the accuracy of pressure measurement is affected by experimental errors, the accuracy of the proposed pressure scales, as well as deviation from the underlying assumptions in the establishment of the pressure scale.

Ruoff *et al.* proposed a method to determine absolute pressure based on simultaneous measurements of length and ultrasonic travel times for isotropically compressed materials.<sup>6</sup> Using this method, the transition pressure of mercury at 0 °C has been successfully determined at 0.76 GPa. Although later studies have succeeded in extending ultrasonic measurements to higher pressures under gas or liquid pressure media,<sup>7,8</sup> the lack of direct length measurement had prohibited absolute pressure determination in these high-pressure devices. Therefore, secondary pressure calibrant or separate calibration experiments had to be pursued for pressure measurements.

Ultrasonic measurements in a multianvil apparatus using

solid pressure medium have been successfully conducted to  $P > 14$  GPa and  $T > 1300$  °C.<sup>9,10</sup> Under such high-pressure and high-temperature conditions, traditional methods based on fixed-point pressure calibration failed to provide precise pressure measurement for determination of pressure and temperature dependences of the elastic properties. In addition, accurate velocity measurements can only be assured if direct length measurement is available, especially in the cases when the sample undergoes phase transformation or plastic deformation.<sup>11,12</sup>

The adaptation of synchrotron x-radiography into the multianvil high-pressure apparatus has facilitated length measurement at high pressure and high temperature. The state-of-the-art ultrasonic measurement using multianvil apparatus utilizes a combination of ultrasonic interferometry, x-ray diffraction, and x-ray radiography techniques, allowing for simultaneous measurements of  $P$ - and  $S$ -wave travel times, specific volume (density), and sample length on either single-crystal or polycrystalline specimens.<sup>12</sup> In these experiments, a combined analysis of ultrasonic velocities and density using finite strain theory provides not only the determination of the elastic moduli and their pressure dependence independent of pressure measurement, but also the absolute pressure. It is worth mentioning that, differing from Ruoff *et al.*,<sup>6</sup> who estimated sample density from the measured length based on linear compression [assuming  $(l/l_0)^3 = (V/V_0) = (\rho_0/\rho)$ ], the density here is determined from x-ray-diffraction data, which are independent of the sample length measurement.

In the following, we briefly describe the experimental implementation. The data analysis using finite strain theory is demonstrated using results on a polycrystalline  $\text{Mg}_2\text{SiO}_4$  wadsleyite collected in a double-stage multianvil apparatus

<sup>a)</sup>Electronic address: baosheng.li@sunysb.edu

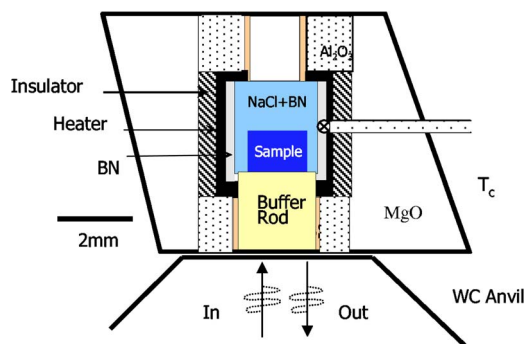


FIG. 1. (Color online) Cross section of the cell assembly used in this study. At the bottom, part of the tungsten carbide anvil (WC) that serves as the external buffer rod is also shown.

(T-25) installed at synchrotron beamline 13-ID-D, GSECARS, Advanced Photon Source (Argonne, IL, USA).<sup>13</sup> The calculated absolute pressures are compared with those obtained from the internal pressure standard based on previous pressure scales of NaCl in the same experiment.

## II. EXPERIMENTAL TECHNIQUES

### A. High-pressure cell assembly

Major components of the experimental setup include the multianvil press, the solid-state detector, the x-ray imaging system, and the ultrasonic measurement system. The detailed layout of these components, installed at 13-ID-D/GSECARS, has been described elsewhere.<sup>11,12</sup> Briefly, the first-stage anvils of the 1000-ton press enclose a cubic cavity, inside of which is the second-stage anvil system of eight tungsten carbide cubes.<sup>13,14</sup> The cubes used in this study are 25.4 mm in linear dimension with one corner truncated into a triangular surface with 4-mm edge length. The truncations enclose an octahedral cavity holding the sample assembly. The diagonally opposite corner of the bottom cube is truncated to provide a lapped surface, on which the transducer is mounted.<sup>9,10</sup> This cube thus serves as an external buffer rod to transmit the acoustic signals to and from the sample cell assembly. Figure 1 shows a cross section of the octahedral sample cell assembly. The sample is placed next to an internal acoustic buffer rod enclosed in the MgO octahedron and is surrounded by a mixture of NaCl plus boron nitride (BN) (NaCl:BN=10:1 by weight). A cylindrical heater made of rhenium foil (25- $\mu\text{m}$  thickness) and a thermal insulator ( $\text{LaCrO}_3$  or  $\text{ZrO}_2$ ) outside the heater are used for experiments at high temperatures. The mixture of NaCl plus BN around the sample serves two important purposes: (1) to provide a pseudohydrostatic pressure environment for the sample and (2) to serve as a secondary pressure standard. During the experiment, x-ray-diffraction patterns from both the sample and the NaCl are collected using energy dispersive x-radiation source at a diffracting angle of  $6.5^\circ$ . These diffraction patterns are analyzed using a full profile fitting procedure (Le Bail method) to obtain the unit-cell parameters from which the unit-cell volume and specific density are derived for equation-of-state analyses.<sup>11,15</sup>

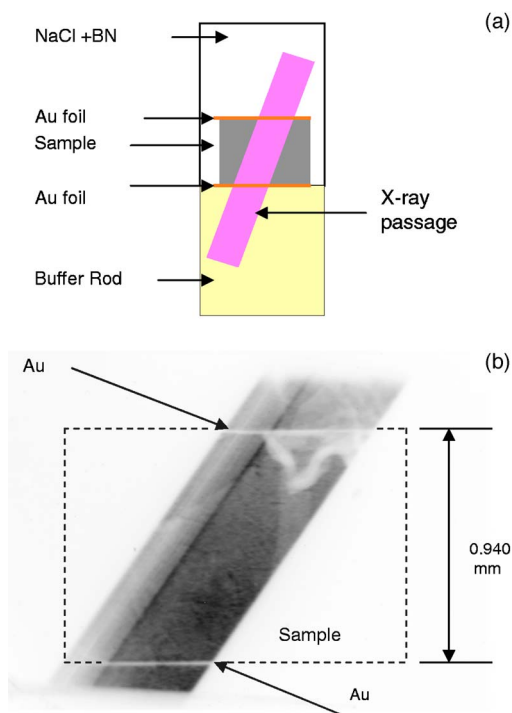


FIG. 2. (Color online) (a) Schematic sample configuration and the x-ray passage. (b) An example of the x-ray image of the sample at high pressure (shown as negative). The dashed line represents the entire sample and the dark region is the part visible by x rays through gaps between WC anvils. The white lines are gold foils placed at both surfaces of the sample.

### B. Ultrasonic interferometry

The acoustic signals are generated and received using disk-shaped dual-mode  $\text{LiNbO}_3$  broadband transducers (20–70 MHz) ( $10^\circ$  Y cut with unspecified polarization direction) so that both  $P$  and  $S$  waves are measured at the same time in a single experiment. At elevated pressures, the transducer remains stress-free since it is located in the gap between the first-stage anvils and the second-stage cubes. Details about the determination of travel times using a transfer function method of ultrasonic interferometry are discussed elsewhere.<sup>11,12,15</sup> It is worth pointing out that the transfer function method, different from the conventional ultrasonic interferometry, collects the entire system response at a wide band of frequencies simultaneously, instead of sweeping through carrier frequencies. Travel times are deduced using the pulse-echo-overlap or phase-comparison method by deconvoluting the system response at discrete frequencies.<sup>12,16</sup>

### C. Sample length measurement

The x-ray imaging system, consisting of a yttrium aluminum garnet (YAG) scintillator and a charge-coupled device (CCD) camera, captures the image of the cell assembly during the high-pressure experiment.<sup>11,12,15</sup> The brightness contrast between the sample and its neighboring regions results from the difference in the x-ray-absorption coefficients of the various materials in the high-pressure cell assembly (Fig. 2). In cases where the sample and its surrounding materials have similar absorption coefficients, metal foils with high x-ray absorption (e.g., gold) are inserted at both the top and bottom surfaces of the sample (see Fig. 2). In high-

pressure ultrasonic measurements, such gold foils (2  $\mu\text{m}$  thick) are routinely used at the sample/buffer rod interface to enhance the mechanical coupling between the buffer rod and sample; these also serve well in delineating the sample boundaries, as seen by the white lines in the invert-contrast image (Fig. 2). To obtain sample lengths at high-pressure and high-temperature conditions, the very last image at the end of the experiment (zero pressure) is used as the reference image to retrieve the change in pixels between neighboring  $P$ - $T$  conditions by cross correlations of the intensity profiles at the center of the sample boundaries. By defining the total pixel number of the sample region in the last image to be the metric length measured by a precise micrometer, sample lengths at high pressure and high temperature are subsequently obtained. Typically, a change of 0.25 pixel can be resolved using cross-correlation method. For a sample with a dimension of about 1000 pixels, a precision to resolve length change at 0.025% can be achieved. By contrast, when the sample dimension in pixels is directly measured from an image, it has a total uncertainty about 2–4 pixels, which gives 0.2%–0.4% in precision, regardless of the sample state at high pressure and high temperature.

#### D. Experimental data

The polycrystalline sample of  $\text{Mg}_2\text{SiO}_4$  wadsleyite used in this study was hot-pressed using the 1000-ton Uniaxial Split-Cylinder Apparatus (USCA-1000) in the High Pressure Laboratory, at Stony Brook at 15 GPa and 1500 K. The sample was confirmed to be homogeneous, fine-grain sized (5–10  $\mu\text{m}$ ), and free of cracks and porosities.<sup>15</sup> Both surfaces of the sample were polished with 1- $\mu\text{m}$  diamond paste finish and parallel within 0.1°. The final sample size used in the ultrasonic experiment was about 2 mm in diameter and  $\sim 1.0$  mm in length. After the sample was assembled into the cell assembly shown in Fig. 1, pressure was first increased to a designated peak value ( $\sim 20$  GPa) at room temperature and then temperature was increased to  $\sim 673$  K to relax the deviatoric stress caused by the solid pressure medium (NaCl + BN) surrounding the sample. After reaching the peak  $P$  and  $T$  conditions, pressure was released slowly and data were collected along decompression at room temperature. The sample recovered from this experiment remained its original length, suggesting that the surrounding NaCl provided a desired pseudohydrostatic condition; the sample had only been subjected to elastic strain during the entire experiment. Details of the results have been described elsewhere.<sup>15</sup> Figure 3 is a summary of the  $P$ - and  $S$ -wave velocities and elastic bulk and shear moduli as a function of density.

### III. RESULTS AND DISCUSSION

#### A. Absolute-pressure determination

Knowing the velocities and density at a series of elastic strains along isothermal conditions, the absolute pressure can be calculated using finite strain equations (1)–(4):<sup>17</sup>

$$P = -3K_{0T}\varepsilon(1 - 2\varepsilon)^{5/2}[1 + 3(4 - K'_{0T})\varepsilon/2], \quad (1)$$

$$K_T = K_{0T}(1 - 2\varepsilon)^{5/2}[1 + (5 - 3K'_{0T})\varepsilon], \quad (2)$$

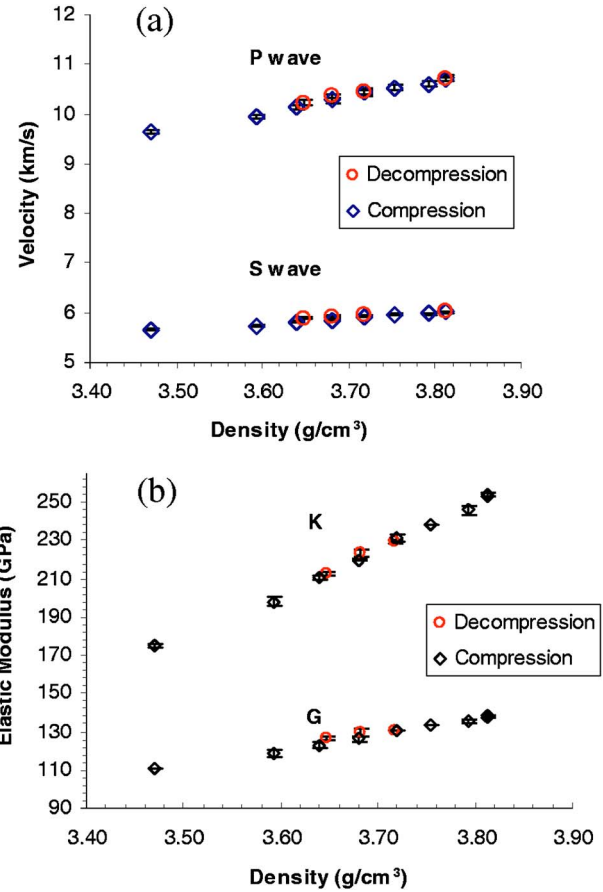


FIG. 3. (Color online) (a)  $P$ - and  $S$ -wave velocities and (b) bulk ( $K$ ) and shear ( $G$ ) moduli of wadsleyite as a function of density. Data collected along compression and on decompression are both shown. Velocities are determined from travel times and sample lengths whereas densities are obtained from x-ray diffraction.

$$K_T = K_S(1 + \alpha\gamma T), \quad (3)$$

$$\varepsilon = 0.5[1 - (\rho/\rho_0)^{2/3}], \quad (4)$$

where  $\varepsilon$  is the Eulerian strain,  $\alpha$  is the thermal expansivity,  $\gamma$  is the Gruneisen parameter, and  $K_T$  and  $K_S$  are the isothermal and adiabatic bulk moduli, respectively. Substituting  $K_T$  with the ultrasonically measured  $K_S$ , Eq. (2) becomes the following:

$$K_S(1 + \alpha\gamma T) = K_{0T}(1 - 2\varepsilon)^{5/2}[1 + (5 - 3K'_{0T})\varepsilon], \quad (5)$$

where the left-hand side represents the isothermal bulk modulus at high pressure. The thermal expansivity and Gruneisen parameter at high pressures are iteratively evaluated using the following equations:

$$\alpha = \alpha_0(0, T) + (\partial\alpha/\partial P)_T P, \quad (6)$$

$$C_P = C_{P0}(0, T) + (\partial C_P/\partial P)_T P, \quad (7)$$

$$(\partial\alpha/\partial P)_T = (\partial K_T/\partial T)_P / K_T^2, \quad (8)$$

$$\gamma = \alpha K_S / \rho C_P, \quad (9)$$

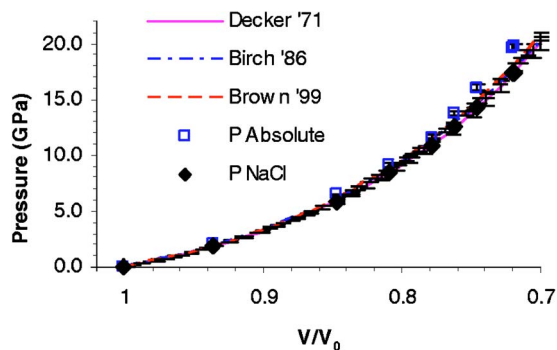


FIG. 4. (Color online) Comparison of pressure as function of the volumetric compressions of NaCl from different pressure scales with the pressures from this study. Empty squares: calculated absolute pressures; solid diamond: pressures from internal pressure standard NaCl and Decker scale in this study.

$$(\partial C_p / \partial P)_T = -T [(\partial \alpha / \partial T)_P + \alpha^2 / \rho]. \quad (10)$$

A least-squares fit to the observed  $K_S$  and strain using Eqs. (2)–(10) yields the optimized  $K_{0T}$  and  $K_{0T'}$  from which the sample pressure can be subsequently calculated using Eq. (1). Evaluation of the variation in Grüneisen parameter at high pressure requires knowledge of  $\alpha_0$ ,  $C_{P0}$ , and  $(\partial K_T / \partial T)_P$  from previously published data, whereas the values of  $(\partial \alpha / \partial P)_T$  and  $(\partial C_p / \partial P)_T$  are calculated and updated iteratively using the thermodynamic relations (8) and (10) during data processing. In practice, since  $\alpha \gamma T$  is so small (on the order of  $10^{-2}$  for most minerals) over a wide pressure range at room temperature, the Grüneisen  $\gamma$  can be estimated either by  $\gamma \rho = \text{const}$  or simply assume  $\gamma$  is constant without causing significant errors in the fitted results (less than the uncertainty). If high-temperature data are available, both  $\alpha_0$  and  $(\partial K_T / \partial T)_P$  can be refined together with  $K_T$  and  $K_{0T'}$ . Alternatively, for room-temperature data, one can use a simplified approach in which the observed  $K_S$  is used directly in Eq. (2) to constrain  $K_{0S}$  and  $(\partial K_S / \partial P)_T$  at ambient conditions.<sup>18</sup> These results, however, need to be converted to the isothermal values using thermoelastic parameters  $\alpha_0$ ,  $\gamma$ , and  $(\partial K_T / \partial T)_P$  before calculating pressure using Eq. (1).

For clarity, in the following discussion, we refer the pressures obtained using x-ray-diffraction data on NaCl and the Decker pressure scale<sup>3</sup> as the “NaCl pressure” and those calculated from Eq. (1) as “absolute pressure.”

## B. Comparison of NaCl pressure and absolute pressure

The pressure determined using Eq. (1) as a function of the compression of NaCl is compared with published NaCl scales in Fig. 4. The errors in pressure scales are obtained from the uncertainties claimed in the respective original studies. The standard deviations in the absolute pressure are obtained by error propagation analysis taking into account the errors in density (volume), bulk modulus, and their pressure derivatives, yielding  $\Delta P = 0.14$  GPa at 10 GPa and 0.23 GPa at 20 GPa. With increasing pressure, the absolute pressures show increased deviation from the NaCl pressure scales, especially at pressures above 5 GPa, the discrepancy appears to exceed the mutual uncertainties. This could be

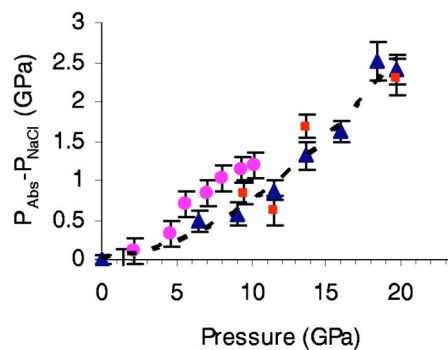


FIG. 5. (Color online) Difference between the absolute pressure and that obtained from Decker NaCl scale as a function of pressure. Solid circles: data from study on (MgFe)O; solid triangles and squares: data from measurements on wadsleyite.

related to the fact that 5 GPa is the maximum pressure of the static compression data that are used to constrain NaCl pressure scales, beyond which shock-wave data are used.<sup>3–5</sup> Figure 5 plots the difference between NaCl pressure and the absolute pressure as a function of pressure, showing that the pressures based on Decker NaCl scale underestimate the sample pressure (absolute pressure) throughout the pressure range, with a maximum error of 2.3 GPa [ $\sim 12.0(1.2)\%$ ] at 20 GPa.

Ruby pressure scale is calibrated against NaCl scale up to 20 GPa, and it is expected to be identical to the NaCl scale within the claimed uncertainty (3%). However, Zha *et al.* calculated absolute pressures using Brillouin scattering and x-ray-diffraction data on San Carlos olivine under quasi-hydrostatic compression and found that the ruby pressure scale overestimated pressures by 2%–3% in the pressure range of 0–32 GPa.<sup>18</sup> On the other hand, using similar techniques to the current study at pressures up to 12 GPa, measurements on other materials have consistently shown results consistent with the notion of the current study on the discrepancy between NaCl pressure and absolute pressure.<sup>19–21</sup> As an example, results from a study on (MgFe)O are included in Fig. 5. Note that in these experiments, data at room temperature are collected after heating/annealing the sample cell assembly in order to minimize the effect of deviatoric stress. In the case of (MgFe)O, the sample assembly is heated to temperatures as high as 1273 K (see details in Ref. 21). Thus, the nonhydrostatic stresses are believed to be released,<sup>22</sup> and the assumption of pressure continuity at the sample–NaCl interface is likely to be satisfied. Additional evidences from peak-width analysis on the sample (wadsleyite) as well as from stress evaluation using NaCl x-ray-diffraction data also suggest that the deviatoric stress in the sample assembly is insignificant. Thus, the discrepancy shown in Fig. 5 may mainly reflect the inaccuracy of the pressure scales due to the lack of experimental constraints in the moderate pressure range during the establishment of the NaCl pressure scales.<sup>3–5</sup> On the other hand, if the assumption of pressure continuity fails at the sample–NaCl interface because of the nonzero shear strength of the solid pressure medium, the observed discrepancy between NaCl pressure and the absolute pressure in Fig. 5 could be largely attributed to the difference of the stress state between the sample and NaCl, in

addition to the uncertainty of NaCl pressure scale in use. To test this, one needs x-ray-diffraction data at multiple diffracting angles using a two-dimensional (2D) detector in conjunction with current experimental setup: feasibility studies have been demonstrated in a recent study.<sup>23</sup> Direct measurements on pressure standard materials, such as NaCl, MgO, and Pt, will provide the opportunity to establish absolute pressure scales that can be used for pressure calibration in high-pressure experiments. Nonetheless, the observed discrepancy between NaCl pressure and the absolute pressure cannot be reconciled by mutual uncertainties and remains to be further investigated.

#### IV. CONCLUDING REMARKS

Using simultaneously measured *P*- and *S*-wave velocities and specific volume in conjunction with finite strain theory, the absolute pressure in multianvil high-pressure experiment has been determined to 20 GPa. The results indicate that the pressures inferred from the equation of state of the surrounding NaCl pressure medium underestimate the sample pressures by 10%–12% up to 20 GPa even after the sample assembly is thermally annealed. Consequently, when the pressures inferred from the NaCl pressure medium are used in equation-of-state analysis, underestimated bulk moduli at high pressures and overestimated pressure derivative will result. In the cases of geophysical application, one might encounter difficulty to interpret the seismic observations using laboratory experimental results.<sup>24</sup> Until further results become available, the calculated absolute pressures in these experiments are believed to be the more accurate measurement of the effective pressure imposed on the sample than those inferred from NaCl based on previous pressure scales.

#### ACKNOWLEDGMENTS

The authors would like to thank I. Jackson for his helpful discussion and comments during the preparation of this manuscript. This research was supported by National Science Foundation under Grant No. EAR000135550 to B.L. The experiment on (MgFe)O was also supported in part by NSF grant to RCL under Grant No. EAR9980451. These experiments were performed at GeoSoilEnviroCARS (Sector 13), Advanced Photon Source (APS), Argonne National Laboratory. GeoSoilEnviroCARS is supported by the National Science Foundation–Earth Sciences (EAR-0217473), Depart-

ment of Energy–Geosciences (DE-FG02-94ER14466) and the State of Illinois. Use of the APS was supported by the U.S. Department of Energy, Basic Energy Sciences, Office of Energy Research, under Contract No. W-31-109-Eng-38. Mineral Physics Institute Publication No. 356.

- <sup>1</sup>A. Onodera and A. Ohtani, *J. Appl. Phys.* **51**, 2581 (1980).
- <sup>2</sup>R. J. Zeto and H. B. Vanfleet, *J. Appl. Phys.* **40**, 2227 (1969).
- <sup>3</sup>D. L. Decker, *J. Appl. Phys.* **42**, 3239 (1971).
- <sup>4</sup>F. Birch, *J. Geophys. Res.* **91**, 4949 (1986).
- <sup>5</sup>J. M. Brown, *J. Appl. Phys.* **86**, 5801 (1999).
- <sup>6</sup>A. L. Ruoff, R. C. Lincoln, and Y. C. Chen, *J. Phys. D* **6**, 1295 (1973).
- <sup>7</sup>I. Jackson and H. Niesler, in *High Pressure Research: Application to Earth and Planetary Sciences*, edited by M. Manghni and Y. Syono (Terra Scientific Publishing Co., Tokyo, 1982), pp. 93–113.
- <sup>8</sup>A. Yoneda, *J. Phys. Earth* **38**, 19 (1990).
- <sup>9</sup>B. Li, G. Chen, G. D. Gwanmesia, and R. C. Liebermann, in *Properties of Earth and Planetary Materials at High Pressure and Temperature*, edited by M. H. Manghni and T. Yagi (American Geophysical Union, Washington DC, 1998), pp. 41–61.
- <sup>10</sup>R. Knoché, S. L. Webb, and D. C. Rubie, in *Properties of Earth and Planetary Materials at High Pressure and Temperature*, edited by M. H. Manghni and T. Yagi (American Geophysical Union, Washington DC, 1998), pp. 119–128.
- <sup>11</sup>J. Kung, B. Li, R. C. Liebermann, Y. Wang, and T. Uchida, *Phys. Earth Planet. Inter.* **147**, 27 (2004).
- <sup>12</sup>B. Li, J. Kung, and R. C. Liebermann, *Phys. Earth Planet. Inter.* **143–144**, 559 (2004).
- <sup>13</sup>T. Uchida *et al.*, *J. Phys.: Condens. Matter* **44**, 11517 (2002).
- <sup>14</sup>R. C. Liebermann and Y. Wang, in *High Pressure Research: Application to Earth and Planetary Sciences*, edited by Y. Syono and M. Manghni (Terra Scientific, Tokyo, 1992), pp. 19–31.
- <sup>15</sup>B. Li, J. Kung, Y. Wang, and T. Uchida, in *Frontier in High Pressure Research: Geophysical Applications*, edited by J. Chen, Y. Wang, T. Duffy, G. Shen, and L. Dobrzinetskaya (Elsevier, New York, in press).
- <sup>16</sup>B. Li, K. Chen, J. Kung, R. C. Liebermann, and D. J. Weidner, *J. Phys.: Condens. Matter* **14**, 11337 (2002).
- <sup>17</sup>F. Birch, *J. Geophys. Res.* **83**, 1257 (1978).
- <sup>18</sup>C. S. Zha, T. S. Duffy, R. T. Downs, H. K. Mao, and R. J. Hemley, *Earth Planet. Sci. Lett.* **159**, 25 (1998).
- <sup>19</sup>K. M. Woody, M.S. thesis, State University of New York at Stony Brook, 2004.
- <sup>20</sup>J. Liu, Ph.D. thesis, State University of New York at Stony Brook, 2000.
- <sup>21</sup>J. Kung, B. Li, D. J. Weidner, J. Zhang, and R. C. Liebermann, *Earth Planet. Sci. Lett.* **203**, 557 (2002).
- <sup>22</sup>Y. Wang, D. J. Weidner, and Y. Meng, in *Properties of Earth and Planetary Materials at High Pressure and Temperature*, edited by M. H. Manghni and T. Yagi (American Geophysical Union, Washington DC, 1998), pp. 365–372.
- <sup>23</sup>Y. Wang and T. Uchida, *Proceedings of the 27th International Thermal Conductivity Conference and Proceedings of the 15th International Thermal Expansion Conference*, Knoxville, Tennessee, 26–29 October 2003, edited by H. Wang and W. Porter (DEStech, Lancaster, PA, 2004), pp. 538–553.
- <sup>24</sup>T. Irfune *et al.*, *Science* **279**, 1698 (1998).